Mechanism of enhanced light emission from an emitting layer embedded in metal-insulator-metal structures

Shinji Hayashi,* Akimichi Maekawa, Suk Chan Kim, and Minoru Fujii
Mesoscopic Materials Laboratory, Department of Electrical and Electronics Engineering, Graduate School of Engineering, Kobe University, Rokko, Nada, 657-8501 Kobe, Japan
(Received 26 April 2010; revised manuscript received 2 July 2010; published 28 July 2010)

Photoluminescence spectra of a dye layer placed at the middle of a metal-insulator-metal (MIM) structure are measured and compared with those of a reference sample without metallic layers. The observed spectra are much sharper than those of the reference sample and the peak wavelength shifts to shorter wavelengths as the observation angle increases. Furthermore, the enhancement in both the emission intensity and power is clearly observed. Electromagnetic calculations based on a point dipole model indicate that the observed light emission is mediated by radiative surface-plasmon polaritons and lowest-order transverse electric modes supported by the MIM structure. The observed enhancement is thought to result from a combination of the enhanced spontaneous emission rate and concentration of radiation intensities in a relatively narrow wavelength region brought by the MIM structure.

DOI: 10.1103/PhysRevB.82.035441 PACS number(s): 78.66.Bz, 78.55.Kz, 78.67.Pt

I. INTRODUCTION

Surface-plasmon polaritons (SPPs) are the coupled modes of collective oscillations of free electrons in a metal and electromagnetic waves that propagate along a metal-insulator interface and decay exponentially away from the interface. Basic properties of SPPs are well understood today[1–3] and recent considerable advances in nanotechnology have opened a new research field called plasmonics,[4,5] which apply SPPs and localized surface plasmons in metallic small particle to fabricate a variety of metal-based optical nanodevices including passive waveguides,[6] active switches, biosensors,[7] and lithography masks, etc. As discussed in detail by Economou[8] early in 1969, one of the physical aspects of SPPs that is very important for the applications is coupling of SPPs propagating at different interfaces. For a sufficiently thin metal film surrounded by insulators, i.e., insulator-metal-insulator (IMI) structure, it is well known that the coupling of SPP modes at the two interfaces results in two SPP modes, known as long- and short-range modes.[1–3,5,6] The long-range mode has a long propagation length and lead to an idea of realizing plasmonic waveguides. Although the propagation length varies considerably depending on the metal and insulator used, metal film thickness and wavelength,[6,9,10] typical values predicted theoretically and confirmed experimentally are on the order of several hundreds of micron for a 15-nm-thick Ag film at the wavelength of 632.8 nm.[11–13] Another structure that supports coupled SPP modes and has attracted a great deal of attention recently is a structure consisting of a thin insulator layer sandwiched with metals, i.e., metal-insulator-metal (MIM) structure.[14–22] Theoretical analyses[16,18–20] have shown that an antisymmetric coupled SPP mode has a waveguide mode character and persists even when the insulator thickness approaches zero; this means that there is no cutoff thickness. In practical applications, imperfections in the structure such as the interface roughness may fix a lower bound of the insulator thickness. However, this mode is very much suited to make plasmonic slot waveguides with nanometer-size insulator cores and has been the subject of intensive theoretical and experimental investigations.[16–22] MIM waveguides with SiO_2 cores as thin as 3.3 nm have been fabricated and their optical properties were investigated in detail both experimentally and theoretically.[17,18] Very recently, negative refraction at visible frequencies was experimentally demonstrated by using specially tailored MIM waveguides.[23] The negative refraction is realized in the wavelength region where the dispersion curve of the antisymmetric SPP mode shows a negative slope.

In addition to the antisymmetric SPP mode, an MIM structure supports a symmetric SPP mode. This SPP mode has a dispersion curve that extends continuously from the radiative to the nonradiative region. Economou[8] called this mode radiative surface-plasmon oscillation. Although the radiative symmetric SPP mode received less attention compared to the antisymmetric SPP mode, the existence of the mode results in interesting optical properties of the MIM structure. When the metallic layers are thin enough, coupling of the mode with light in air makes nominally opaque MIM structures highly transparent in a relatively narrow wavelength region.[24] This property has recently been applied to realize color-tunable light-emitting devices.[25] Omnidirectional light emission from a blue-emitting polymer layer sandwiched by Au films was reported by Liu and Brongersma.[26] Attempts to increase the light extraction efficiency of organic light-emitting diodes by introducing MIM structures have also been reported.[27–30] Although the improvement in the light-extraction efficiency has been observed and explained in terms of microcavity effects, the physical mechanism of the enhanced light emission from the MIM structure has not yet been clarified.

In this work, we explore photoluminescence (PL) properties of a dye layer embedded in the MIM structure. We demonstrate clearly the enhancement of PL intensities and emitted power relative to those of the dye layer embedded in a reference sample without metal layers. With the aid of electromagnetic calculations based on a point dipole model, we show that the observed peculiar properties of PL spectra and

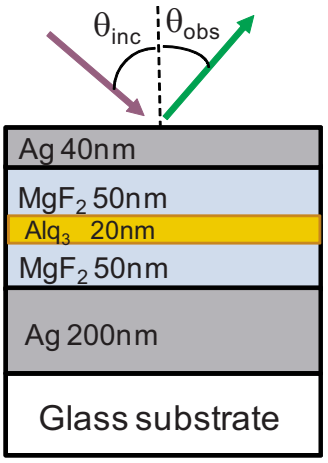

FIG. 1. (Color online) Structure of MIM sample prepared.

the enhancement can be well explained by the light emission mediated by the radiative SPP mode of the MIM structure. This paper is organized as follows. In Sec. II, following the description of experimental procedures, we present experimental results. In Sec. III, after identifying the electromagnetic modes responsible for the light emission from the MIM structure, the mechanism of the PL enhancement is discussed in detail with the aid of results of electromagnetic calculations. Finally, we give our conclusions in Sec. IV.

II. EXPERIMENTAL RESULTS

MIM structures schematically shown in Fig. 1 were prepared by vacuum evaporation. First, a 200-nm-thick Ag film is deposited on a glass substrate. On top of the Ag film an insulator layer consisting of a 20-nm-thick tris(8-hydroxyquinoline) aluminum (Alq_3) film sandwiched with 50-nm-thick MgF_2 films was deposited. Finally, a 40-nm-thick Ag film was deposited to complete the MIM structure. The thicknesses of the films were monitored by a quartz microbalance. Transmission and reflection spectra revealed that the top Ag film is a continuous film not consisting of island particles. As a reference sample, a sample without Ag films was also prepared. To measure PL spectra, the sample was mounted on a rotating table and excited by a laser beam with a wavelength of 408 nm from a laser diode. The incident light was *s* polarized and the incident angle was set at 65°. Light emitted from the sample at an angle θ_{obs} was collected by a fiber optic cable and sent to a 25 cm single monochromator equipped with a charge-coupled device. The head of the fiber optic cable with an aperture of 1.5 mm in diameter (corresponding to a solid angle of $\sim 10^{-4}$ sr^{-1}) was mounted on a rotating arm and the observation angle was controlled by a computer. In front of the aperture a polarizer was inserted to select the polarization of emitted light. PL spectra were measured by varying θ_{obs} from 0 to 90° with a step of 1°.

In Figs. 2(a)–2(c), unpolarized, *p*- and *s*-polarized PL spectra obtained with various θ_{obs} are shown, respectively. Spectra obtained for the reference sample with $\theta_{obs}=0°$ are also presented after multiplying the raw intensities by a factor of 5. The MIM sample exhibits relatively sharp peaks which shift to shorter wavelengths as θ_{obs} increases, while the reference sample exhibits broad PL bands which stay almost at the same position. The broad PL spectra of the reference sample are very similar to those of Alq_3 amorphous films prepared by vacuum deposition.[31,32] The spectra are redshifted relative to those of Alq_3 solutions, indicating that the molecules are densely packed in the amorphous films. As seen for the unpolarized spectrum obtained with $\theta_{obs}=36°$, unpolarized spectra are split into two peaks for $\theta_{obs} > \sim 30°$. A close comparison between Figs. 2(a)–2(c) reveals that the long-wavelength peaks in the doublets are *p* polarized and the short-wavelength peaks are *s* polarized. It should be noted that although PL is detected through the top opaque Ag film, the PL peak intensities of the MIM sample are very much enhanced relative to those of the reference sample. We define the PL enhancement factor (EF) as the ratio of the PL intensity of the MIM sample to that of the reference sample. The PL EF for unpolarized spectra obtained from the results presented in Fig. 2(a) are plotted in Fig. 3(a). We see that the maximum EF of ~25 is achieved for $\theta_{obs}=0°$ and EF decreases as θ_{obs} increases.

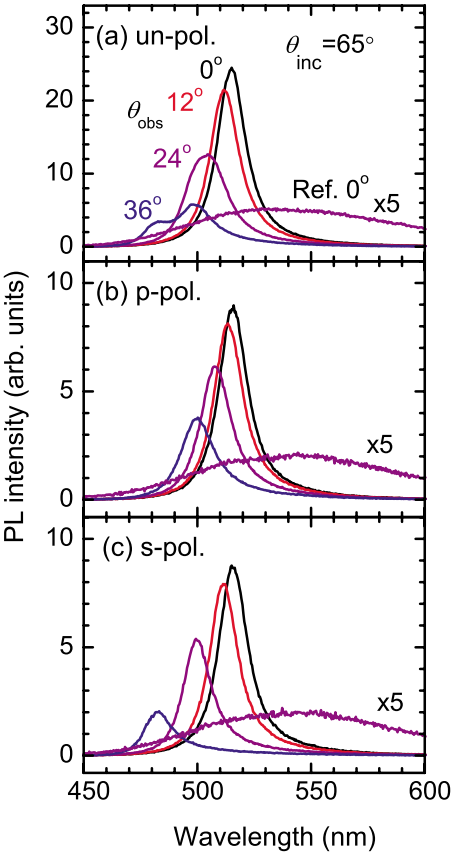

FIG. 2. (Color online) (a) Unpolarized, (b) *p*-polarized, and (c) *s*-polarized spectra obtained for MIM and reference samples.

Unpolarized spectra similar to those presented in Fig. 2(a) were measured for $0° \leq \theta_{obs} \leq 90°$ with a step of 1°. From the results we estimated the power radiated into the half space at the air side of the sample. Since the radiation pattern can be assumed to have a rotational symmetry around the normal axis of the sample, the power radiated into the half

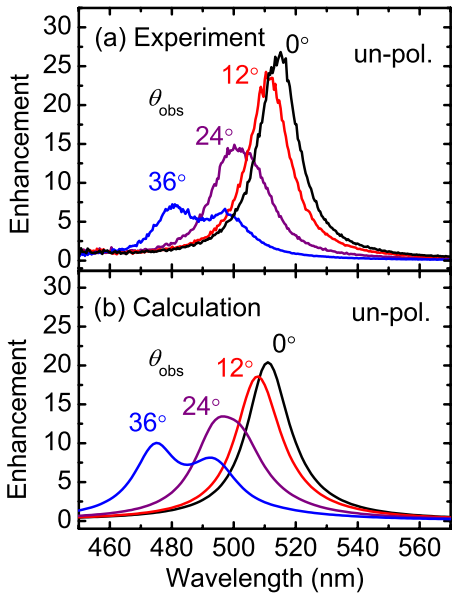

FIG. 3. (Color online) (a) Enhancement factor obtained by dividing MIM spectra by reference spectra. (b) Calculated PL enhancement factor for various θ_{obs}.

space is given by $P=2\pi\int_0^{\pi/2}S(\theta)\sin\theta d\theta$, where $S(\theta)$ is the power radiated into a unit solid angle element in the direction specified by θ_{obs}. The intensities of the measured spectra are proportional to $S(\theta)$ and all the spectra obtained were thus multiplied by sin θ and summed up. Figure 4(a) shows the integrated spectra of the MIM and reference samples and the power EF obtained by taking the ratio. We see that the integrated spectrum of the MIM sample is still very sharp compared to that of the reference sample. Furthermore, the emitted power of the MIM sample are enhanced in the wavelength region between ~470 and ~520 nm. We see that the power EF takes a maximum value of ~2.5 around 500 nm. The experimental results presented here clearly demonstrate

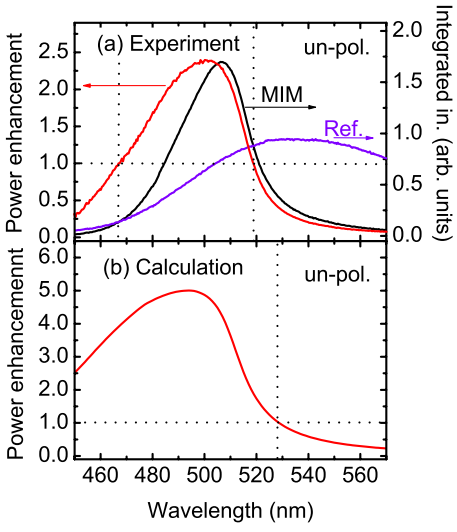

FIG. 4. (Color online) (a) Integrated unpolarized spectra for MIM and reference samples and power enhancement factor. (b) Calculated power enhancement factor.

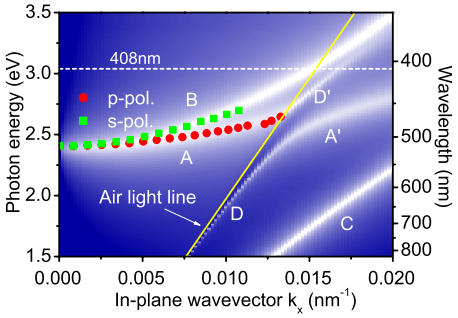

FIG. 5. (Color online) Calculated dispersion curves and experimental points obtained from PL spectra.

that the MIM structure greatly modifies the PL properties of the dye layer and leads to the enhancement in both the intensity and the emitted power, even though the light is emitted through the opaque top Ag layer.

III. COMPARISON WITH THEORETICAL CALCULATIONS AND DISCUSSION

A. Electromagnetic modes mediating the light emission

As shown in Fig. 2, the PL peak observed for the MIM sample shifts to shorter wavelengths as θ_{obs} increases. This shift is thought to be the manifestation of the dispersion of electromagnetic modes of the MIM structure mediating the light emission. The relationship between the peak wavelength λ_p and the observation angle θ_{obs} was converted into that between the photon energy E and in-plane wave vector k_x by using a relation $k_x=\frac{2\pi}{\lambda_p}\sin\theta_{obs}$. The results for p and s polarization are plotted in Fig. 5 and compared with theoretical dispersion curves described below.

As explained in detail in previous papers,[26,33] calculation of power dissipated by an oscillating dipole placed in multilayer systems allows one to obtain the dispersion curves of electromagnetic modes supported by the systems. In our calculations, the sample structure shown in Fig. 2 is assumed and an oscillating point dipole is located in the middle of the Alq_3 layer. An isotropic orientation of the dipole was assumed. Literature values of the dielectric functions for Ag,[34] MgF_2,[35] and Alq_3[36] were used. In Fig. 5, whiter regions correspond to higher power dissipation and represent dispersion curves. In order to facilitate the assignment of the dispersion branches, we present in Fig. 6 the dispersion curves obtained for a simpler MIM structure consisting of a 135-nm-thick MgF_2 layer sandwiched with semi-infinite Ag layers. We note that the dispersion curves presented in Fig. 6 are very similar to those presented in Fig. 2(f) in Ref. 21. Referring to previous studies[8,14,16,21,37] we can assign the three branches seen in Fig. 6 to the antisymmetric SPP, symmetric SPP, and TE_0 (lowest-order transverse electric) modes, respectively, as indicated in the figure. The symmetric SPP mode is also labeled as TM_0 (lowest-order transverse magnetic) mode. Since the electric fields associated with the TM_0 and TE_0 modes are confined in the insulator layer, they are also classified into waveguide modes. From a comparison with Fig. 6, it is straightforward to assign the dispersion branches A, B,

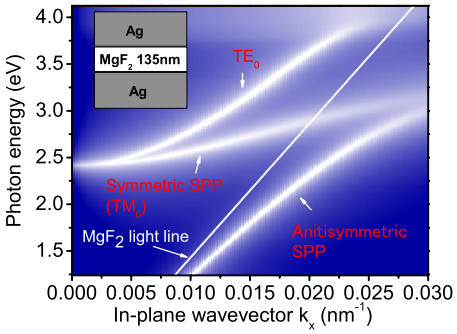

FIG. 6. (Color online) Dispersion curves obtained for Ag-MgF_2(135 nm)-Ag structure.

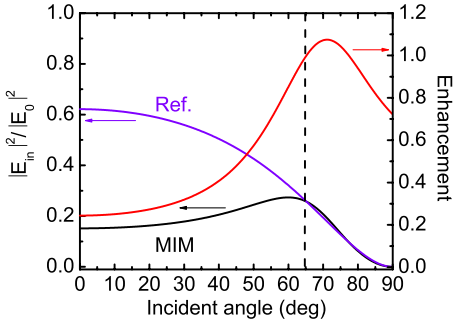

FIG. 7. (Color online) Calculated intensities of incident field for MIM and reference samples and enhancement factor for incident field.

and C in Fig. 5 to the TM_0, TE_0, and antisymmetric SPP mode, respectively. Since the top Ag layer in the sample structure has a finite thickness, a SPP mode at the air-Ag interface also appears in this figure as labeled as branch D. This branch intersects with the TM_0 branch around $k_x = 0.014$ nm^{-1} and $E = 2.6$ eV. The hybridization of the branches at the crossing point generates a gap[37] and after the gap the air-Ag SPP branch further goes up (branch D′) and the TM_0 branch tends to be flat as k_x increases (branch A′). We see that the experimental points determined from the *p*- and *s*-polarized PL spectra are in excellent agreement with the dispersion curves of the TM_0 mode and the TE_0 mode. The agreement allows us to conclude that *p*-polarized light emission presently observed is mediated by the TM_0 mode while *s*-polarized light emission is mediated by the TE_0 mode.

B. Mechanism of PL enhancement

In discussing the mechanisms of PL enhancement caused by metallic nanostructures, it is very common to consider separately the enhancement in the excitation and emission processes.[38] We consider first the excitation process based on a point dipole model. When the excitation light is incident on the multilayer sample, as a consequence of the multiple reflections, an electric field distribution is settled in the Alq_3 layer. The interaction of the dipole with the incident field is described by $|\mathbf{E}_{in} \cdot \mathbf{p}_a|^2$, where $\mathbf{p}_a$ is an absorption dipole and $\mathbf{E}_{in}$ is the electric field generated by the incident light at the position of the dipole. When the random orientation of the dipole is assumed, the excitation rate is proportional to $|\mathbf{E}_{in}|^2$.

We have calculated $|\mathbf{E}_{in}|^2$ at the middle of the Alq_3 for both the MIM and reference samples by using the 2×2 transfer matrix method. As in the experiments, *s*-polarized incident light with a wavelength of 408 nm was assumed. Figure 7 shows the calculated curves of $\frac{|\mathbf{E}_{in}|^2}{|\mathbf{E}_0|^2}$ as a function of the incident angle, where $|\mathbf{E}_0|$ is the amplitude of the incident light. The enhancement factor of the incident field obtained by the ratio of the MIM result to that of the reference is also plotted. We see that the field intensity of the reference sample decreases monotonously as the incident angle increases while that of the MIM sample takes a maximum around 60°. The field-enhancement factor takes a maximum value of ~1.1 around 70°. Returning to Fig. 5 we note that the horizontal line corresponding to the wavelength of incident light (408 nm) intersects with the dispersion curve of TE_0 mode. Therefore, the peak in the field intensity in the MIM sample and also in the enhancement factor can be attributed to the resonant excitation of the TE_0 mode by the incident light. However, the maximum enhancement factor is not large. This is due to a large imaginary part of the dielectric constant of Alq_3 around 408 nm (absorption region). The result shown in Fig. 7 suggests that in the present experiment made with an incident angle of 65° the field-enhancement factor is ~1.0 and the observed PL enhancement is due to the enhancement in the emission process.

For the sake of comparison, we calculated the incident field intensity also for structures without the bottom Ag layer, i.e., MI structure, and without the top Ag layer, i.e., IM structure. The results indicate that, in contrast to the MIM structure, the field EF of these structures depends weakly on the incident angle and does not show a pronounced peak. This is due to the absence of the resonant mode in these structures at the wavelength of the incident light (408 nm). The field EF obtained for the MI structure is very small (less than 0.161), because the incident light is strongly attenuated in the top Ag layer. On the other hand, the field EF obtained for the IM structure is ~2.0. This high EF results from the constructive interference between the incident light and the light reflected at the IM interface. As far as the enhancement in the excitation channel is concerned, our numerical results suggest that the IM structure is more advantageous than the MIM structure, although the EF in the emission channel is smaller than that of the MIM structure as discussed later.

In the discussion of emission processes, we also assume a point dipole placed in the middle of the Alq_3 layer oscillating at the frequency of emitted light. The emission process in the present MIM structure can qualitatively be explained in the following manner. An oscillating dipole generates the electromagnetic fields (dipole radiation), which can be regarded as the superposition of plane waves having various in-plane wave vectors.[39] When the frequency and in-plane wave vector match those of the modes in the MIM structure, these modes are excited. Since the TE_0 and TM_0 modes are radiative and can couple with light in air, what is observed is the decay of the excited modes into light in air. Therefore, for a fixed observation angle, i.e., for a fixed in-plane wave vector, a PL peak appears at a photon energy (wavelength) determined by the dispersion curve.

Electromagnetic theories of radiation by an oscillating dipole embedded in a multilayer system have been developed by several authors.[39–42] According to Neyts,[42] the intensity of light emitted into a unit solid angle in the observation direction is given by

$$P_{dipole}(\lambda,\theta_{obs}) = \frac{1}{(1-q)+qF}\frac{dP(\lambda,\theta_{obs})}{d\Omega}, \qquad (1)$$

where $\frac{dP(\lambda,\theta_{obs})}{d\Omega}$ is the power density per solid angle $d\Omega$, F is the total power supplied by the dipole, and q is a quantum efficiency of the emitter. $\frac{dP(\lambda,\theta_{obs})}{d\Omega}$ and F are normalized to the total power emitted by the dipole in an infinite medium embedding the dipole, i.e., Alq_3 in the present case. Explicit expressions of $\frac{dP(\lambda,\theta_{obs})}{d\Omega}$ and F are found in Ref. 42 and can be calculated from the reflection and transmission Fresnell coefficients at the interfaces in the multilayer system.

In calculating $P_{dipole}(\lambda,\theta_{obs})$, we used a literature value of $q=0.25$.[32] We also assumed that the magnitude of the oscillating dipole is independent of the wavelength. This assumption resulted in flat spectra for the reference sample rather than the experimental broad peak seen in Fig. 2. In order to compare with experimental results, we took the ratio of calculated spectra of $P_{dipole}(\lambda,\theta_{obs})$ for the MIM sample to those of the reference sample. The intensity EF so obtained for various θ_{obs} is displayed in Fig. 3(b). It can be seen that the calculated results reproduce fairly well the peak position and magnitude of enhancement of the experimental results shown in Fig. 3(a). However, a close comparison between Figs. 3(a) and 3(b) reveals that calculated EF are smaller than experimental ones for small θ_{obs} while calculated ones are larger for large θ_{obs}. By integrating the intensity spectra over θ_{obs}, we obtained the power emitted into the half space at the air side for both the MIM and reference sample. The power EF obtained by taking their ratio is plotted in Fig. 4(b). It can be seen that the maximum EF of ~5 is achieved around $\lambda=490$ nm. Our calculation shows that around $\lambda=490$ nm, the power emitted into the half space normalized to the total power emitted into an infinite Alq_3 medium is ~0.10 for the reference sample, while that for the MIM sample is ~0.50, leading to the power EF of ~5. As is well known, the power extracted from an emitter embedded in a medium with a high refractive index is limited to a small value because the total reflection prohibits the light transmission into a low index material.[33,43] This is the case for the reference sample. On the other hand, the TM_0 and TE_0 modes in the MIM structure provide channels to transmit the emitted light into the outside of the structure and the fraction of the emitted power is increased up to ~0.50 even with the absorption loss in the top Ag layer.

A comparison between Figs. 4(a) and 4(b) reveals that the spectrum of calculated power enhancement reproduces qualitatively the experimental spectrum. However, the maximum EF achieved experimentally is about a half of the calculated one and the experimental enhancement factor in the short-wavelength region is much smaller than the calculated one. The reason for the discrepancy is not clear at present, but the discrepancy may arise from the oversimplification of the calculation model. In fact, the observed PL intensity is not determined by a point dipole placed in the middle of the Alq_3 layer but by excited molecules distributed in a 20-nm-thick Alq_3 layer. Roughness of the interfaces in the multilayer system may also influence the intensity and angular distribution of the PL intensity, which are not taken into account in the calculations. Nevertheless, calculations based on the simple model reproduce semiquantitatively the experimental results.

We note here that the spontaneous emission rate calculated for a point dipole embedded in the MIM structure is enhanced in the wavelength region where the TM_0 and TE_0 modes exist. A maximum enhancement of ~40% is obtained around $\lambda=490$ nm. This is a manifestation of so-called Purcell effect,[44] in which the TM_0 and TE_0 modes provide high photonic mode densities. The great modification in the emission spectra and the enhancement observed are thought to arise from a combination of the Purcell effect and concentration of emission intensities in a relatively narrow wavelength region brought by the TM_0 and TE_0 modes.

We finally comment on the intensity and power EF calculated for the MI and IM structures. They are almost independent of the observation angle and show monotonous dependence on the wavelength in the region considered here (between 450 and 570 nm). These results are again due to the absence of electromagnetic modes mediating the light emission in the MI and IM structures. For the MI structure, both the intensity and power EF decrease as the wavelength increases and take values smaller than 0.1. The small values are caused by the strong attenuation of emitted light in the top Ag layer. For the IM structure, the intensity EF increases from 2.4 to 3.5 when the wavelength increases from 450 to 570 nm while the power EF increases from 2.5 to 4.1. The enhancement in the IM structure results from the constructive interference between the light directly emitted from the dipole and that reflected at the IM interface. Since the maximum values of the intensity and power EF for the MIM structure [Figs. 3(b) and 4(b)] are larger than the above values of the EF for the IM structure, we can conclude that the MIM structure is more advantageous than the IM structure to obtain the enhancement in the emission process in the wavelength region where the TM_0 and TE_0 modes mediate the light emission. The MIM structure is thus effective to increase the light-extraction efficiencies in the organic-light-emitting diodes driven by current injection. It should be noted that the emission wavelength of the MIM structure can easily be controlled by changing the thickness of the insulator layer, since the TM_0 and TE_0 dispersion curves move to lower photon energies as the thickness increases.

In the case of excitation by light, even after taking into account the incident field EF of ~2.0 for the IM structure, values of PL EF for the MIM structure at the emission peaks [Fig. 3(b)] are larger than those for the IM structure by at least a factor of 2. The power EF for the IM structure after multiplication of the incident field EF varies from ~5.0 to ~8.2 as the wavelength varies from 450 to 570 nm while that of the MIM structure takes a maximum value of ~5.0 around $\lambda=490$ nm and decreases rapidly as the wavelength increases [Fig. 4(b)]. From these results, we can suggest that the MIM structure is more suited for realizing PL with high intensities in a relatively narrow wavelength region while the IM structure is effective for realizing PL with high powers over a wide wavelength region.

IV. CONCLUSION

We have shown that the intensities and power of PL from the Alq_3 layer embedded in the MIM structure are enhanced relative to those in the reference sample without metallic layers. The maximum enhancement factor achieved is ~25 for the intensity and ~2.5 for the power. Although the PL enhancement is possible in the excitation and emission processes, our theoretical analysis indicates that the enhancement in the emission processes is dominant. A good agreement between experimental and theoretical dispersion curves allows us to conclude that the enhanced PL is mediated by the TE_0 and TM_0 modes specific to the MIM structure. The calculation based on a point dipole model reproduces semiquantitatively the observed enhancement factor. The present experimental and theoretical results clearly demonstrate that TE_0 and TM_0 modes in the MIM structure play important roles in determining the emission properties of embedded emitters. Although the enhancement in the light-extraction efficiency in MIM organic-light-emitting diodes was simply mentioned as due to the microcavity effects, the present study reveals the physical origins of the enhancement. It is straightforward to apply the present findings to optimize the performance of light-emitting devices.

ACKNOWLEDGMENTS

This work was supported in part by a grant-in-aid for scientific research (C) (Grant No. 20613009) from the Ministry of Education, Culture, Sports, Science and Technology of Japan.

*hayashi@eedept.kobe-u.ac.jp

[1] V. M. Agranovich and D. L. Mills, *Surface Polaritons* (North-Holland, Amsterdam, 1982).
[2] A. D. Boardman, *Electromagnetic Surface Modes* (Wiley, Chichester, 1982).
[3] H. Raether, *Surface Plasmons on Smooth and Rough Surfaces and on Gratings*, Springer Tracts in Modern Physics Vol. 111 (Springe-Verlag, Berlin, 1988).
[4] R. Zia, J. A. Schuller,A. Chandran, and M. L. Brongersma, Mater. Today **9**, 20 (2006).
[5] M. L. Brongersma and P. G. Kik, *Surface Plasmon Nanophotonics*, Springer Series in Optical Sciences Vol. 131 (Springer, Dordrecht, 2007).
[6] S. I. Bozhevolnyi, *Plasmonic Nanoguides and Circuits* (Pan Stanford, Singapore, 2009).
[7] J. Homola, *Surface Plasmon Resonance Based Sensors*, Springer Series on Chemical Sensors and Biosensors Vol. 4 (Springer, Berlin, 2006).
[8] E. N. Economou, Phys. Rev. **182**, 539 (1969).
[9] D. Sarid, Phys. Rev. Lett. **47**, 1927 (1981).
[10] S. A. Maier and H. A. Atwater, J. Appl. Phys. **98**, 011101 (2005).
[11] Y. Kuwamura, M. Fukui, and O. Tada, J. Phys. Soc. Jpn. **52**, 2350 (1983).
[12] A. E. Craig, G. A. Olson, and D. Sarid, Opt. Lett. **8**, 380 (1983).
[13] H. Dohi, Y. Kuwamura, M. Fukui, and O. Tada, J. Phys. Soc. Jpn. **53**, 2828 (1984).
[14] F. Villa, T. Lopez-Rios, and L. E. Regalado, Phys. Rev. B **63**, 165103 (2001).
[15] P. A. Hobson, W. L. Barnes, D. G. Lidzey, G. A. Gehring, M. S. Skolnik, and S. Walker, Appl. Phys. Lett. **81**, 3519 (2002).
[16] J. A. Dionne, L. A. Sweatlock, H. A. Atwater, and A. Polman, Phys. Rev. B **73**, 035407 (2006).
[17] H. T. Miyazaki and Y. Kurokawa, Phys. Rev. Lett. **96**, 097401 (2006).
[18] Y. Kurokawa and H. T. Miyazaki, Phys. Rev. B **75**, 035411 (2007).
[19] F. Kusunoki, T. Yotsuya, and J. Takahara, Opt. Express **14**, 5651 (2006).
[20] J. Takahara and F. Kusunoki, IEICE Trans. Electron., **E90-C**, 87 (2007).
[21] L. H. Smith, M. C. Taylor, I. R. Hooper, and W. L. Barnes, J. Mod. Opt. **55**, 2929 (2008).
[22] M. J. Preiner, K. T. Shimizu, J. S. White, and N. M. Melosh, Appl. Phys. Lett. **92**, 113109 (2008).
[23] H. J. Lezec, J. A. Dionne, and H. A. Atwater, Science **316**, 430 (2007).
[24] D. Y. Lei and H. C. Ong, Appl. Phys. Lett. **91**, 211107 (2007).
[25] J. Feng, T. Okamoto, J. Simonen, and S. Kawata, Appl. Phys. Lett. **90**, 081106 (2007).
[26] J. S. Q. Liu and M. L. Brongersma, Appl. Phys. Lett. **90**, 091116 (2007).
[27] H. Peng, X. Zhu, J. Sun, Z. Xie, and S. Xie, Appl. Phys. Lett. **87**, 173505 (2005).
[28] H. Peng, J. Sun, X. Zhu, X. Yu, M. Wong, and H.-S. Kwok, Appl. Phys. Lett. **88**, 073517 (2006).
[29] N. A. Reinke, C. Ackermann, and W. Brütting, Opt. Commun. **266**, 191 (2006).
[30] S. Nowy, B. C. Krummacher, J. Frischeisen, N. A. Reinke, and W. Brütting, J. Appl. Phys. **104**, 123109 (2008).
[31] M. Brinkmann, G. Gadret, M. Muccini, C. Taliani, N. Masciocchi, and A. Sironi, J. Am. Chem. Soc. **122**, 5147 (2000).
[32] V. V. N. Ravi Kishore, K. L. Narasimhan, and N. Periasamy, Phys. Chem. Chem. Phys. **5**, 1386 (2003).
[33] W. L. Barnes, J. Lightwave Technol. **17**, 2170 (1999).
[34] E. D. Palik, *Handbook of Optical Constants of Solids* (Academic Press, Orlando, 1985).
[35] E. D. Palik, *Handbook of Optical Constants of Solids II* (Academic Press, Sandiego, 1991).
[36] L. H. Smith, J. A. E. Wasey, D. W. Samuel, and W. L. Barnes, Adv. Funct. Mater. **15**, 1839 (2005).
[37] G. Chen, G. A. Smolyakov, S. R. J. Brueck, and K. J. Malloy, Opt. Express **16**, 14902 (2008).
[38] P. Anger, P. Bharadwaj, and L. Novotny, Phys. Rev. Lett. **96**, 113002 (2006).
[39] J. Enderlein, Chem. Phys. **247**, 1 (1999).
[40] R. R. Chance, A. Prock, and R. Silbey, Adv. Chem. Phys. **37**, 1 (1978).
[41] W. Lukosz, J. Opt. Soc. Am. **71**, 744 (1981).
[42] K. A. Neyts, J. Opt. Soc. Am. A **15**, 962 (1998).
[43] J. A. E. Wasey and W. L. Barnes, J. Mod. Opt. **47**, 725 (2000).
[44] W. L. Barnes, J. Mod. Opt. **45**, 661 (1998).